Efficient Modelling of Near-Wall Turbulence in Hybrid RANS-LES Simulations

Marius Herr[1,2(✉)] and Axel Probst[2]

[1] TU Braunschweig, Hermann-Blenk-Str. 37, 38108 Braunschweig, Germany
m.herr@tu-bs.de
[2] DLR (German Aerospace Center), Bunsenstr. 10, 37073 Goettingen, Germany
axel.probst@dlr.de

Abstract. This study investigates the applicability and efficiency potential of analytical wall functions in conjunction with hybrid RANS-LES methods in two unstructured flow solvers, i.e. the compressible DLR-TAU code and the incompressible DLR-THETA code. Wall-modelled LES simulations of a periodic channel flow using IDDES confirm the validity of the wall-function approach over a broad range of grids with $12.5 \leq y^+(1) \leq 210$. For the more complex separated flows over a backward facing step and a wall-mounted hump, DDES simulations show that $y^+(1)$ has to be limited to 25 regardless of the flow solver, in order to achieve agreement with results using full near-wall resolution. Despite that restriction, the computing time can be reduced by up to $2/3$ compared to the fully-resolved case.

Keywords: Hybrid RANS-LES · Wall functions · DLR-TAU · DLR-THETA

1 Introduction

Combining the Large-Eddy Simulation (LES) methodology with the statistical RANS modelling approach enables to perform locally scale-resolving simulations of aeronautical flows for high, flight-relevant Reynolds numbers. Despite the efficiency advantage of such hybrid RANS-LES methods (HRLM) compared to pure LES, this approach remains computational-intensive and time-consuming for the specified scope of application [9]. This is due to the high demand on the wall-normal grid resolution for no-slip walls requiring a so-called *low-Re* grid with $y^+(1) \leq 1$, where $y^+(1)$ denotes the wall-adjacent cell-height normalized in wall units.

Coupling the HRLM approach with wall-functions (HRLM-WF), however, allows to avoid the highly-resolved near-wall region by replacing the no-slip condition with a more sophisticated *high-Re* boundary condition and modelling the effects of the unresolved near-wall flow by analytical wall laws. Gritskevich et al. [3] investigated a HRLM approach with common RANS wall-functions by means of various internal flow test cases and confirmed the basic validity of this simulation method. In this work, we adopt the universal wall-function method of Knopp et al. [5] in numerical studies with the compressible flow solver TAU and the incompressible solver THETA in order to systematically explore the applicability of different HRLM-WF models, based on

A. Dillmann et al. (Eds.): STAB/DGLR Symposium 2020, NNFM 151, pp. 615–624, 2021.
https://doi.org/10.1007/978-3-030-79561-0_58

variants of Detached-Eddy Simulation (DES). Despite similarities of TAU and THETA with respect to the underlying data structures and numerical schemes, fundamental differences are present with regard to the near-wall grid metric (cf. Sect. 2). Hence an applicability of HRLM-WF for both flow solvers is non-trivial and might depend on different criteria for each code. Therefore, after a fundamental exploration of HRLM-WF by means of a periodic channel flow (Sect. 3.1), the approach is analysed separately by TAU and THETA on the basis of the backward facing step (Sect. 3.2) and the NASA wall mounted hump (Sect. 3.3).

2 Numerical Method

The compressible TAU code and the incompressible THETA code are unstructured 2nd-order finite-volume solvers developed by DLR. Both solvers use specialized numerical methods for their respective Mach-number regimes, but they share the same *dual-cell* approach to support identical so-called *primary* grids with mixed cells (e.g. tetrahedra, hexahedra). In scale-resolving simulations such as hybrid RANS-LES, both codes use low-dissipative central schemes for the convective fluxes, which were shown to yield satisfying accuracy for various flow cases [8]. Note that the low-Mach preconditioning available in TAU allows for solving low-speed flow problems, too, despite lower computational efficiency compared to THETA.

Another important difference between TAU and THETA concerns the location of the first off-wall control point, where the flow variables and also the wall function are evaluated: while in TAU this point simply corresponds to the first off-wall cell vertex of the primary grid, THETA introduces an additional *shifted* point at about 0.27 times the height of the first grid cell. This actually increases the near-wall resolution on a given primary grid and reduces the *effective* value of $y^+(1)$, which is therefore denoted as $y_e^+(1)$ for THETA in the subsequent comparisons with TAU.

2.1 Hybrid RANS-LES Modelling

To assess the combination of wall functions with hybrid RANS-LES we consider two well-known variants of Detached-Eddy Simulation (DES): first, the Delayed DES (DDES) [10] which discerns between RANS mode in attached flow and LES mode in detached areas based on the local grid resolution and a boundary-layer (*RANS shielding*) sensor. Second, the Improved DDES (IDDES) [9] which extends the DDES by wall-modelled LES capabilities for partly-resolved attached boundary layers, e.g. downstream of separation or synthetic-turbulence injection.

While IDDES is needed to simulate the periodic channel, DDES is considered sufficient for flows with local resolved separations, i.e. the backward-facing step and the wall-mounted hump. In those test cases, however, the common approach to build 3D meshes by extruding 2D meshes in lateral direction, can delay the onset of resolved turbulence in the initial free shear layers [7]. As a remedy, we employ a vorticity-sensitive LES-filter width, $\tilde{\Delta}_\omega$ [7], instead of the classic maximum-length filter of DES. The Spalart-Allmaras one-equation model serves as RANS background model.

2.2 Analytical Wall Function Approach

The low-Re approach, which is usually applied to the near-wall RANS regions in HRLM, requires a complete resolution of the boundary layer up to the viscous sublayer with $y^+(1) = 1$. In order to relax this strict requirement on the wall-normal grid resolution, we combine the HRLM-models with the analytical wall-function approach by Knopp et al. [5]. The applied wall-functions have been derived from the incompressible RANS momentum equation. This method blends well-known wall laws, i.e. Spalding (F_{Sp}^{-1}), Reichhardt (F_{Rei}) and the logarithmic law of the wall $\left(F_{\mathrm{Log}}\right)$, such that corresponding RANS results are widely independent of the first cell height $y^+(1)$:

$$F_{\mathrm{Sp}}^{-1} = u^+ + 8.43\left(e^{0.41u^+} - \sum_{n=0}^{5}\frac{(0.41u^+)^n}{n!}\right), \quad F_{\mathrm{Log}} = \frac{\ln(y^+)}{0.41} + 5.1 \tag{1}$$

$$F_{\mathrm{Rei}} = \frac{\ln(1+0.4y^+)}{0.41} + 7.8\left(1 - e^{-\frac{y^+}{11}} - \frac{y^+}{11}e^{-\frac{y^+}{3}}\right) \tag{2}$$

The blending between these laws is designed in line with solutions of the respective turbulence model on low-Re meshes, so that a model-consistent universal wall function formulation is achieved, see [5] for details. On this basis the wall shear stress τ_w is computed for a given $y^+(1)$ and is being prescribed at solid walls. Thus, the previous no-slip boundary condition ($u_w = 0$) is being replaced by a Neumann boundary condition ($\tau_w \propto \frac{\partial u}{\partial y}\big|_{y=0}$). Since such wall functions were originally designed for steady RANS computations, it is non trivial that this approach works for instationary HRLM simulations, too. Nevertheless, the mostly stationary character of the near-wall RANS region in HRLM, as well as the successful application of similar wall functions by [3] justify this approach at least for low values of $y^+(1)$.

Numerical Correction for Wall-Function Computations in THETA. Despite the universal formulation of the wall functions one observes significant skin-friction errors in high-Re computations with TAU or THETA on grids with the first off-wall grid point located in the buffer layer around $y^+(1) \approx 5 \ldots 15$, similar to the findings in [4]. The reason lies in numerical errors in the momentum diffusion (relying on second velocity derivatives) at the first off-wall cell face of such coarse grids which, however, become only relevant in the lower, high-curvature buffer region, where diffusion plays a dominant role.

As an ad-hoc remedy, the relative error of the discretized diffusion term can be quantified as a function of $y_e^+(1)$ by comparison with a fine (*low-Re*) grid and transformed into an empirical correction function ϕ_{corr} for the diffusion. So far, such a correction has only been derived for THETA, whose special near-wall metric prevents a direct transfer to other solvers. It is realized via an additional momentum source at the first off-wall cell face, using the *thin-shear layer approximation* of the wall-normal diffusion and an interpolated look-up table for ϕ_{corr}.

3 Results

3.1 Periodic Channel

For a basic validation of the wall function approach in conjunction with HRLM-based wall-modelled LES, a periodic channel flow at $Re_\tau = u_\tau \delta / \nu \approx 4179$ [6] is computed with TAU using IDDES. The channel geometry comprises the height 2δ, length $2\pi\delta$ and width $\pi\delta$. Periodic boundary conditions are applied in stream- and spanwise directions, and a momentum source term is applied to keep the corresponding target bulk Reynolds number constant at $Re_\delta = U_0 \delta / \nu = 98300$, as given by DNS data [6]. For this setting the wall-adjacent RANS areas exhibits a wall normal thickness of about $0.05\,\delta$. The LES mode is active in the remaining region. A structured grid with hexahedral cells is applied, with grid spacings of $\Delta x = 0.1\delta$ (streamwise) and $\Delta z = 0.05\delta$ (lateral). For the temporal discretisation a normalized time step of $\Delta t^+ = 0.4$ is used, overall corresponding to the setup given in [8].

The low-Re mesh with $y^+(1) \approx 1$ serves as reference mesh for the wall-function simulations. For the high-Re meshes $y^+(1)$ is varied systematically over a range from 12.5 to 210. Except for $y^+(1) = 210$, where a homogeneous meshing strategy is applied, the meshes exhibit a wall-normal growth factor of 1.14. For the high-Re meshes the total cell number can be reduced from 39.6 % for $y^+(1) = 12.5$ up to 61.4 % for $y^+(1) = 52.5$ (cf. Fig. 1 right). The total simulations time amounts to $30 l/U_0$ with the channel length l and the bulk velocity U_0, where a time span of $20 l/U_0$ is used to calculate temporal statistics. Figure 1 left presents TAU-IDDES results in terms of mean velocity profiles, where good agreement between the low- and high-Re solutions over the entire range of $y^+(1)$ can be stated. The largest, but still moderate deviation with respect to Re_τ is present for $y^+(1) = 12.5$ (cf. Fig. 1 right), which may be attributed to the discretisation errors in the momentum diffusion, as described in Sect. 2.2. Besides, all present simulations share small deviations from the DNS around $y^+ \approx 500$, i.e. above the RANS-LES interface, indicating a remainder of the well-known *log-layer mismatch* issue of wall-modelled LES [9].

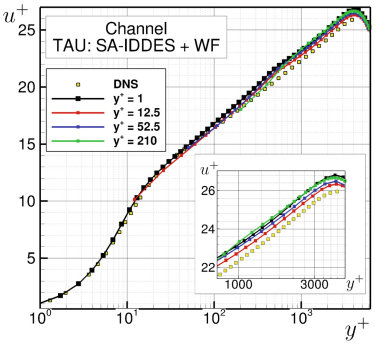

$y^+(1)$	# cells	red. of cells	Re_τ	dev. Re_τ
1	$4.27 \cdot 10^5$	-	4026	-
12.5	$2.58 \cdot 10^5$	39.6 %	4092	+1.6 %
52.5	$1.65 \cdot 10^5$	61.4 %	4069	+1.1 %
210	$1.73 \cdot 10^5$	59.4 %	4046	+0.5 %

Fig. 1. DLR-TAU IDDES results of the periodic channel flow for $Re_\delta = 98.300$ [6]: Velocity profiles for different $y^+(1)$ (left) and overview of mesh properties with averaged values of Re_τ (right).

3.2 Backward-Facing Step

The backward-facing step (BFS) represents a more complex test case including geometry-induced flow separation and reattachment. We consider the experimental flow studies by Driver and Seegmiller [1] with a Reynold number of $Re_h = 37,500$ based on the step height h and a Mach number of 0.13, using DDES in a similar numerical setup as [8]. Periodic boundary conditions are applied at the spanwise domain borders which are separated by a distance of 4 h. At the inflow a partially-developed turbulent boundary layer with a thickness as in the experiment is prescribed. The RANS mode, which is active for attached boundary layers, exhibits a thickness of about 1 h for $x < 0$ and reduces to approx. 0.1 h behind the separation.

We employ hybrid meshes with a mostly unchanged, hex-dominated unstructured area located in the LES region downstream of the step, whereas structured areas with varying $y^+(1)$, but constant wall-normal expansion factor of $r = 1.15$, are located close to the walls. In all grids 68 extrusion layers are used to resolve the spanwise domain. As reference for the DDES-WF simulations, a low-Re mesh is created, which fulfils $y^+(1) < 1$ at all wall-adjacent cells. To analyse the impact of $y^+(1)$ on the flow solution, meshes with $y^+(1)$ values of 12.5, 25 and 50, referring to the streamwise position $x/h = -1$, were built. The corresponding wall distances $y(1)$ at this position were applied for all wall-adjacent cells which leads to a suboptimal design of the high-Re grids in the vicinity of the step, exhibiting large cell-volume ratios at the hybrid interface (cf. Fig. 2). Compared to the low-Re grid, the total cell reduction ranges from 24.5 % for $y^+(1) = 12.5$ (resp. 34.1 % for $y_e^+(1) = 13.5$ using THETA) to 34.1 % for $y^+(1) = 50$ (resp. 62.4 % for $y_e^+(1) = 50$).

The physical time step of $dt = 0.07\,h/U_0$ ensures $\mathrm{CFL}_{conv} < 1$ (i.e. CFL-number based on the convection velocity) within the whole LES region. The total simulation time is $300\,h/U_0$, where $200\,c/U_0$ are used to obtain time-averaged results.

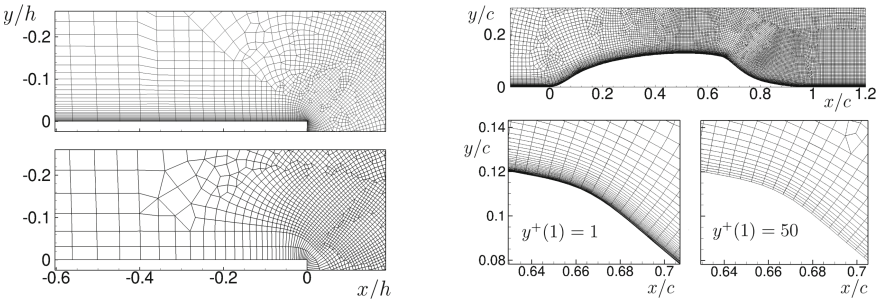

Fig. 2. Left: Mesh comparison of the 2-D backward-facing step. Top view: low-Re mesh with $y^+(1) = 1$. Bottom view: high-Re mesh with $y^+(1) = 50$. Right: 2D-cut of NASA wall-mounted hump discretised with hybrid meshing strategy.

Figure 3 shows skin-friction distributions along the step computed with TAU and THETA using DDES-(WF) on the described grids, together with reference data from the experiment [1] and RANS (Spalart-Allmaras model). Be reminded that for a given grid, the internal THETA grid metric leads to lower *effective* first cell heights than TAU, thus denoted as $y_e^+(1)$. Also note that along the entire x-axes very good agreement between the low-Re solutions of both flow solvers and the experimental data is achieved, which demonstrates the benefit of scale-resolving approaches compared to RANS in massively-separated flow.

Concerning the high-Re results from TAU in Fig. 3 (left), smaller values of $y^+(1)$ lead to a better agreement with the low-Re solution in the recirculation area ($x/h > 0$ and $c_f < 0$), pointing out the limits of DDES-WF for $y^+(1) > 25$ in this challenging flow. Concerning the recovery region downstream of reattachment ($x/h \approx 5.5$), all results become more similar and nearly align at the outflow plane. For $x/h < 0$ the best results are obtained for $y^+ = 25$, whereas the skin friction is overestimated for $y^+(1) = 12.5$ (due to the discretisation errors described in Sect. 2.2), but surprisingly also not matched for $y^+(1) = 50$. The latter remains an open issue which was not further analysed because of the overall large deviations for this mesh.

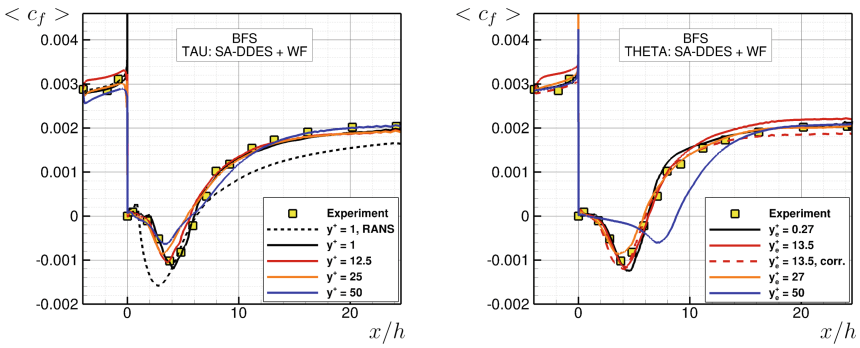

Fig. 3. Mean skin-friction results for the backward-facing step at Re = 37,500: DLR-TAU solutions for different values of $y^+(1)$ (left) and results computed with DLR-THETA and a corrected verion of THETA (right).

Analysing the c_f-curves computed by THETA in Fig. 3 (right), similar trends as for TAU are observed within the recirculation, i.e. better agreement with the low-Re solution is achieved for decreasing values of $y_e^+(1)$. The results for $y_e^+(1) = 50$, however, which corresponds to a *primary* grid with $y^+(1) = 185$, demonstrate the limits of the high-Re approach on very coarse meshes, as the separated region is drastically over-predicted. Figure 3 (right) also illustrates that the deviations for $y_e^+(1) = 13.5$ and $x < 0$ can indeed be traced back to near-wall discretisation errors, since a much better agreement with $y^+(1)$ is achieved with the diffusion correction (*corr.*) mentioned in Sect. 2.2, without interfering with the already good prediction in the recirculation region. As an intermediate summary for this challenging separated flow case, $y^+(1)$ for TAU or $y_e^+(1)$

for THETA should not exceed values of 25 in order to obtain satisfying agreement with the low-Re solutions.

3.3 NASA Wall-Mounted Hump

Another typical and challenging HRLM test case is the NASA wall-mounted hump [2], cf. Fig. 2 (right). Except for the slip-wall condition at the upper wall, the same boundary conditions as for the backward-facing step are applied. At the lower wall, the prescribed inflow matches a boundary layer with $Re_\theta \approx 7200$ from a precursor RANS simulation. The domain length, height, and crest height equal $6.14\,c$, $0.905\,c$ and $0.128\,c$, respectively, where c is the hump chord length. The spanwise extension amounts to $0.4\,c$ which is considered large enough to obtain span-independent flow solutions. With $Re_c = 936.000$ (based on c and the inflow velocity U_0) and $Ma = 0.1$ both compressible and incompressible simulations are possible. The thickness of the wall-adjacent RANS layer is $0.03\,c$ before the separation and reduces to $0.003\,c$ behind it. As for the BFS, a hybrid grid with structured near-wall regions and a hex-dominated unstructured mesh in the separation region is applied. This allows a high local resolution in the latter area, where Δx and Δy are approximately $0.005\,c$. The low-Re mesh fulfils $y^+(1) < 1$ at all wall-adjacent cells and is stretched by $r = 1.15$ in wall-normal direction. For the high-Re meshes (also $r = 1.15$), $y^+(1)$ equals 12.5, 25 and 50 at the crest position at $x = 0.5$, cf. Fig. 2 (right). Refer to Table 1 for the corresponding grid-point savings, as well as the $y_e^+(1)$-values for THETA. The total simulation time equals $30\,c/U_0$ ($20\,c/U_0$ are used for temporal statistics) with a time step size of $dt = c/500U_0$, so that $\mathrm{CFL}_{conv} < 1$ is fulfilled in the LES region.

Figure 4 compares DDES-(WF) skin-friction profiles for the two flow solvers, TAU (left) and THETA (right), with varying $y_{(e)}^+(1)$. For both solvers, high deviations between the low-Re solution and experimental data exist in the area of flow separation. This is due to the grey area at the RANS-LES interface, which remains critical in this flow despite using a modified filter width as remedy, cf. Sect. 2.1. In such regions the production of resolved turbulence is delayed resulting in an unphysical stable shear layer with too low initial turbulent shear stress $< u'v' >$, cf. Fig. 5 (right).

Considering the TAU skin friction profiles, similar findings as for the BFS are made: First, the trend towards better mean skin-friction agreement with the low-Re results for decreasing $y^+(1)$ within the recirculation area. Second, the alignment of profiles in the area of reattachment for increasing x/c, and third, the effect of numerical errors for $y^+(1) = 12.5$, yielding an overestimation of c_f at $x/c < 0.66$. Analogue to the previous test case, overall satisfying agreement with the low-Re reference is obtained, if $y^+(1)$ is limited to a value of 25.

Considering the THETA results in Fig. 4 (right), we observe an unexpected effect in the high-Re results that is in contrast to TAU: on the coarsest near-wall grid, i.e. $y_e^+(1) = 27$, the recirculation area is shifted by $0.15\,c$ in upstream direction and agrees remarkably well with the experimental data. This apparent reduction of the grey-area problem is supported by plots of the velocity profiles and the turbulent shear stress at the $x/c = 0.8$, i.e. inside the initial separating shear layer (cf. Fig. 5), where a stronger onset of turbulent stress compared to the low-Re results is visible. Note that TAU's high-Re result shows this behaviour, too, but to a lesser extent that is not sufficient to

alter the mean skin friction. Despite this apparent improvement by using a coarse grid with wall functions, there is no physical reasoning to infer a consistent advantage over the higher-resolved low-Re approach. At this point, we believe it may be triggered by spurious numerical disturbances arising from the wall function method, calling for a more detailed analysis.

Moreover, Fig. 4 (right) includes THETA results for $y_e^+(1) = 13.5$ using the diffusion correction according to Sect. 2.2. As for the BFS, much better agreement with the low-Re result is obtained, without interfering with the prediction of separation.

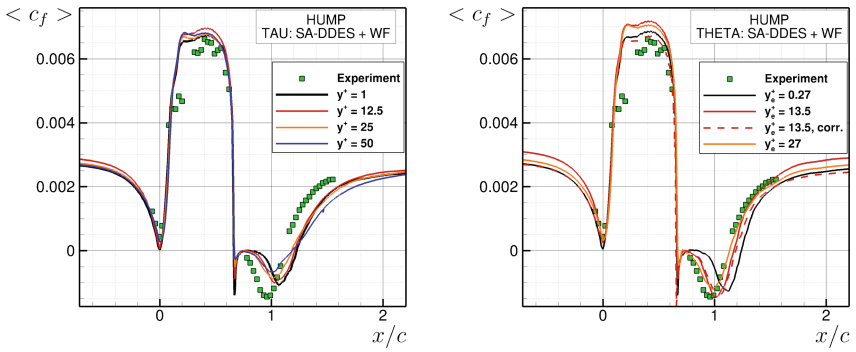

Fig. 4. Mean skin-friction results for the NASA wall-mounted hump at Re = 936.000: DLR-TAU solutions for different values of $y^+(1)$ (left) and results computed with DLR-THETA and a corrected version of THETA (right).

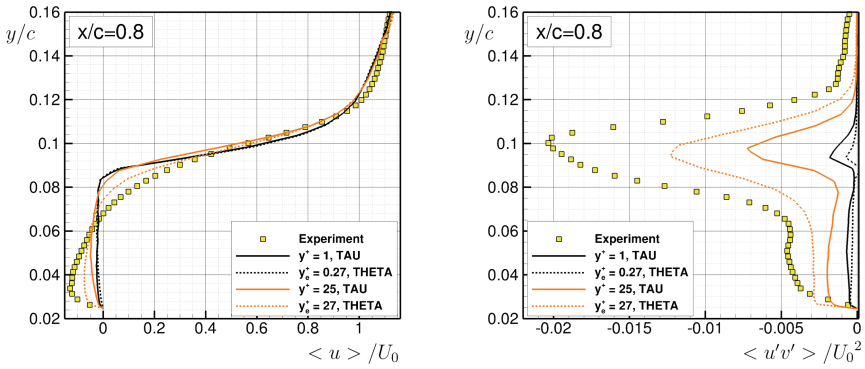

Fig. 5. Profiles of the velocity component in streamwise direction (left) and the normalised shear stress component $< u'w' >$ (right) at position $x/c = 0.8$ for both DLR-TAU and DLR-THETA with experimental data from [2].

3.4 Efficiency Considerations

The reduction of total computing time of high-Re simulations is analysed for the NASA wall-mounted hump. For time integration, TAU utilises a dual-time stepping scheme, i.e. for every physical time step a certain number of inner iterations is calculated. This number is controlled by a set of Cauchy convergence criteria which is kept constant for all simulations. THETA employs a projection scheme with inner linear-solver iterations which are controlled via a fixed residual-reduction threshold.

For TAU, the average time of a single inner iteration can be evaluated separately. Table 1 shows a reduction compared to the low-Re computation up to 36.8 % for $y^+(1) = 50$. In addition, though, the average number of inner iterations is also significantly reduced for increasing values of $y^+(1)$. This is due to the reduced near-wall cell aspect ratio on high-Re meshes, leading to lower numerical stiffness and consequently faster inner convergence of the physical time steps. Considering both effects in combination, one obtains a drastic reduction of total computing time, amounting to 60.4 % for $y^+(1) = 12.5$ and increasing to 72.6 % for $y^+(1) = 50$. For THETA, despite using even coarser meshes for a given $y_e^+(1)$, the overall reduction in computing time is just comparable to TAU. Although the individual effects could not be analysed separately, we assume that the linear-solver convergence in THETA benefits less than TAU from the reduced aspect ratios.

Table 1. Overview of cell and simulation-time reductions on high-Re meshes for the NASA hump.

	$y^+_{(e)}(1)$	red. cells	red. comp. time/it.	red. it./phys. dt	Total red. comp. time
TAU	12.5	28.1 %	25.7 %	46.7 %	60.4 %
	25	33.8 %	31.6 %	51.4 %	66.7 %
	50	38.9 %	36.8 %	56.7 %	72.6 %
THETA	13.5	38.9 %	–	–	61.5 %
	27	44.1 %	–	–	64.4 %

4 Conclusions

The combination of the analytical wall-function approach of Knopp et al. [5] with hybrid RANS-LES methods has been assessed using two different unstructured flow solvers, DLR-TAU and DLR-THETA. With TAU a basic validation of IDDES-WF acting as wall-modelled LES for the periodic channel flow at $Re_\tau \approx 4200$ has shown consistent results with the low-Re solution over a large range of $y^+(1) = 12.5 \ldots 210$. For the separated flows over a backward-facing step and a wall-mounted hump, TAU computations with DDES-WF yield higher demands on the near-wall resolution, i.e. $y^+(1) \leq 25$, in order to match the low-Re reference results in the recirculation regions.

Although this demand is confirmed with THETA, it can be fulfilled with coarser *primary* grids due to THETA's additional internal near-wall point. Moreover, the high-Re results of THETA for the hump show a surprising, yet inexplicable reduction of the grey area, yielding a better agreement with the experiment than the low-Re reference. Finally, a well-known [4] systematic overestimation of the skin friction on high-Re grids with $y^+_{(e)}(1) \approx 12.5$, which was found in all test cases with both flow solvers, could be cured for THETA by an ad-hoc correction of the near-wall momentum diffusion.

With regard to computational efficiency it has been confirmed that wall functions combined with HRLM may provide enormous savings of up to $2/3$ in overall computing time compared to the low-Re HRLM, demonstrating a large potential for future application in high-Reynolds aeronautical flows.

Acknowledgements. We thank Dr. Roland Kessler (DLR Göttingen, now retired) for providing the numerical diffusion correction in THETA.

References

1. Driver, D.M., Seegmiller, H.L.: Features of a reattaching turbulent shear layer in divergent channel flow. AIAA J. **23**(2), 163–171 (1985)
2. Greenblatt, D., Paschal, K.B., Yao, C., Harris, J., Schaeffler, N.W., Washburn, A.E.: Experimental investigation of separation control part 1: baseline and steady suction, AIAA J. **44**(12), 2820–2830 (2006)
3. Gritskevich, M.S., Garbaruk, A.V., Menter, F.R.: A comprehensive study of improved delayed detached eddy simulation with wall functions. Flow Turb Combust **98**(2), 461–479 (2017)
4. Kalitzin, G., Medic, G., Iaccarino, G., Durbin, P.: Near-wall behaviour of RANS turbulence models and implications for wall functions. J. Comp. Phys. **204**(1), 265–291 (2005)
5. Knopp, T., Alrutz, T., Schwamborn, D.: A grid and flow adaptive wall-function method for RANS turbulence modelling. J. Comput. Phys. **220**(1), 19–40 (2006)
6. Lozano-Duran, A., Jimenez, J.: Effect of the computational domain on direct simulations of turbulent channels up to $Re_\tau = 4200$. Phys. Fluids **26**(1), 011702 (2014)
7. Mockett, C., et al.: Two non-zonal approaches to accelerate RANS to LES transition of free shear layers in DES. In: Progress in Hybrid RANS-LES Modelling, Notes on Numerical Fluid Mechanics and Multidisciplinary Design vol. 130, pp. 187–201 (2015)
8. Probst, A., Löwe, J., Reuß, S., Knopp, T., Kessler, R.: Scale-resolving simulations with a low-dissipation low-dispersion second-order scheme for unstructured flow solvers. AIAA J. **54**(10), 2972–2987 (2016)
9. Shur, M.L., Spalart, P.R., Strelets, M.K., Travin, A.K.: A Hybrid RANS-LES approach with delayed-DES and wall-modelled LES capabilities. Int. J. Heat Fluid Flow **29**(6), 406–417 (2008)
10. Spalart, P.R., Deck, S., Shur, M.L., Squires, K.D., Strelets, M.K., Travin, A.K.: A new version of detached-eddy simulation, resistant to ambiguous grid densities. Theor. Comput. Fluid Dyn. **20**(3), 181–195 (2008)